PERGAMON

International Journal of Multiphase Flow 27 (2001) 1397–1414

International Journal of Multiphase Flow

www.elsevier.com/locate/ijmulflow

Investigation of three dimensional interstitial velocity, solids motion, and orientation in solid–liquid flow using particle tracking velocimetry

K.B. Zitoun [a], S.K. Sastry [b,*], Y. Guezennec [c]

[a] *Kerry Ingredients, Woodstock, Ont., Canada N4S 8A4*

[b] *Department of Food, Agricultural and Biological Engineering, The Ohio State University, 590 Woody Hayes Drive, Columbus, OH 43210, USA*

[c] *Robinson Laboratory, Department of Mechanical Engineering, The Ohio State University, 206 W Eighteenth Avenue, Columbus, OH 43210, USA*

Received 18 October 1999; received in revised form 21 January 2001

Abstract

In this study, the advancement of Particle Tracking Velocimetry (PTV) techniques to study flows of coarse solid–liquid mixtures is reported. The method has been adapted successfully to high solid concentrations (30% and 50%) by matching the index of refraction of clear solid pieces and the carrier fluid. Digital image processing of tracer and solid piece motion recorded on stereoscopic motion picture films were used to identify solids and tracers, and obtain data on location and velocity. These studies reveal local slip velocity between phases that is dependent on solid piece shape and aspect ratio. However, the complexity of the flow necessitates the use of unprocessed velocity vector information, rather than a flow field interpolated onto a regular grid. The PTV technique may be further modified to determine solid motions and orientation distribution of high solids suspensions, by determination of Euler angles. Our results demonstrate that objects of non-unity aspect ratio tend to align along the flow, within the constraints set by solids concentration, and that such solids also demonstrate decreased rotational motion in comparison with non-elongated solids. It is noted that elongated solids may rotate till an equilibrium position is achieved, whereupon no further rotation occurs. The results also show that, as expected, increasing solids size and concentration decreases the incidence of rotation.

Keywords: Solid–liquid; Interstitial velocity; Orientation; Particle Tracking Velocimetry

* Corresponding author. Tel.: +1-614-292-3508; fax: +1-614-292-9448.
E-mail address: sastry.2@osu.edu (S.K. Sastry).

0301-9322/01/$ - see front matter
PII: S0301-9322(01)00011-8

1. Introduction

Although the motion of suspended solids in flowing liquids is of interest in many areas of engineering, most literature has considered the conveying of dense, relatively fine particles in the turbulent flow of water. Recent industry interest in sterilization of biomaterials has created new challenges for flow visualization. In such systems, (e.g., Orangi et al., 1998), flows involve solid–liquid mixtures where solids-to-tube diameter ratios are in the range of 0.1–0.3; solids density is typically close to that of the fluid phase, which typically exhibits non-Newtonian behavior, with a high apparent viscosity in the shear rate range of application (Zitoun, 1992; Balasubramaniam, 1993). The heat transfer between the solid and liquid phases in such systems is dependent on the interstitial relative velocities between the phases.

In addition, when electroconductive heating methods are used for sterilization, the flow structure takes on major significance, because the effective electrical conductivity of the suspension depends on the orientation distribution of the solids relative to the flow. Finally, the rotational and translational motions of individual solid pieces are also significant since they result in fluid disturbance and mixing, and consequently, enhanced heat transfer. Each of the above measurement/visualization problems are confounded by the presence of large solids in the flow.

Most methods developed for velocity measurement have been used for mixing and turbulent flow. These can be classified into two categories: optical methods and opaque methods. Most optical methods (i.e., Pulsed Laser Velocimetry (PLV) and Laser Doppler Velocimetry (LDV) methods) cannot be applied to two-phase flow when the particles are large ($D > 1$ cm). For the case of opaque materials, Magnetic Resonance Imaging (MRI) can be used (Manavel et al., 1993) but its three-dimensional intensity distribution using transverse-phase encoding gradient is based on the assumption that the motion of the flow is steady in the statistical sense along the flow direction within the test section (Altobeli et al., 1991; Sinton and Chow, 1991). Also, this MRI method needs knowledge of a general flow direction to get accurate information. Positron Emission Particle Tracking (PEPT) (Broadbent et al., 1993), Computer-Automated Radioactive Particle Tracking (CARPT) (Yang et al., 1993), and Gamma Ray Emission Particle Tracking (γEPT) (Larachi et al., 1995) work with opaque media but involve single particle measurements and suffer from slow data acquisition rates. These experiments consist in letting a particle to flow for 10–12 h until it maps the whole area of interest. This would require a closed vessel or a recirculating system.

Modern developments in image processing have been responsible for the use of flow visualization to arrive at vital quantitative flow velocity information with a high degree of accuracy. Particle Tracking Velocimetry (PTV) is one of the several such tools which were developed over the past decade and have been applied to a variety of fluid mechanics problems (Adrian, 1991; Liu and Adrian, 1993). The advantages are its non-intrusive nature and that full field information can be obtained. PTV has been used in mixing (Venkat et al., 1996), and fluidized beds for gas–liquid–solid mixtures (Chen and Fan, 1992). This method has been used in the past in some of NASA's microgravity experiments (Meyer et al., 1993), in the study of internal combustion engines and turbulent mixing (Trigui et al., 1992, 1994). All previous work that dealt with PTV were for single-phase flows. In this work, we extend traditional PTV techniques to coarse solid–liquid mixtures, using transparent solids that have the same index of refraction as the solution, to measure interstitial velocity at high solid concentration.

The goal of this research is to adapt the PTV technique to solid–liquid mixtures of high solid concentration and high solid to tube size ratio (up to 1:2) to measure the interstitial velocities and the relative velocity between the two phases in upward flow through a vertical tube; characterize the rotational velocities of solid objects in these flows, and determine the solids orientation angle distribution relative to the flow direction.

2. Materials and methods

2.1. Experimental setup

Three dimensional flow visualization requires two cameras which are synchronized or a single camera with a mirror arrangement to get two views of the flow volume of interest, in this case, the flow of large solid pieces in a tube. The test section consisted of a Pyrex tube of 0.0508 m inside diameter and 1.524 m length. The camera-mirror arrangement used in our experiment is shown in Fig. 1. The stereo angle was adjustable from a few degrees (stereo angle associated with human eyes being 6–7°) to orthogonal views (90°), but in the present study was maintained at 90°.

The solid–liquid mixtures were conveyed by air pressure from the inlet. The flow rate was measured and controlled using differential pressure transmitters (Model 1151DP Alphaline, Rosemount, MN).

The tube curvature causes an optical distortion which decreases the extent of the image received by the video camera. This problem was minimized by using the refractive index matching technique. The test section was enclosed in a rectangular box with a plexiglass window of refractive

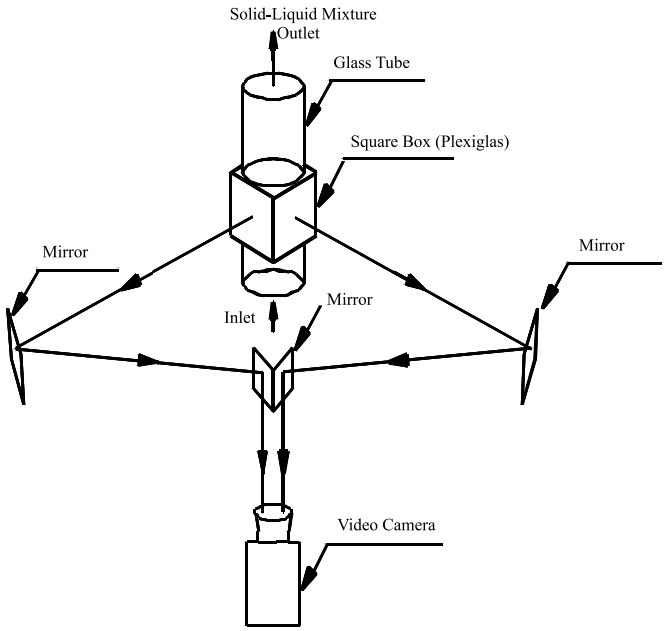

Fig. 1. Experimental setup.

index equal to that of the glass tube (~1.5). The box was filled with the same fluid used for the experiment: sodium carboxymethyl cellulose (CMC), to minimize the curvature effect. After recording the flow, the videotape was replayed, and the frames grabbed, processed and analyzed to determine the velocity vectors. Also, the system was precalibrated in-situ, (see procedures detailed later), to minimize distortion errors.

Image acquisition was accomplished using a CCD camera (S-VHS Panasonic AG 450). The frames were grabbed at 1/30 s using a digital video recorder (Panasonic AG 7350) equipped with search/jog dial and frame grabber board (P360F, Dipix Technologies, Ontario, Canada). The resolution of acquired images was 512×480 pixels, with the field of view being optimized as described later.

2.2. Experimental conditions and test materials

All experiments were conducted at each of two flow rates: 1.577×10^{-4} and 3.154×10^{-4} m^3/s; and two solids concentrations: 30% and 50%. The solids consisted either of cubes of side 8, 16 or 24 mm; or cylinders of 8×8, 8×16, 16×16 and 16×24 mm (diameter $\times$ length in all cases), respectively. The carrier fluids used were aqueous solutions of CMC. Rheological properties were determined by using a coaxial cylinder viscometer (Rheomat Model 115; Contraves Industrial Division; Cincinnati, OH). Results were analyzed based on the Ostwald-de-Waele power law model ($\tau = K\gamma^n$). The values of consistency coefficient (K) and flow behavior index (n) of the carrier fluid were 1.24 Pa s^n and 0.52 for the interstitial velocity and orientation experiments, and 1.31 Pa s^n and 0.53, respectively, for the rotation experiments. The generalized Reynolds numbers for the fluids flowing at the experimental test rates were calculated as 9.3 and 26.5, respectively. Densities of the various experimental materials are presented in Table 1. Each experimental run was repeated five times.

2.3. Experimental procedure: measurement of interstitial fluid velocity

The experiment consisted of introducing a solid–liquid mixture consisting of solid cubic pieces and into the medium at the inlet section, and videotaping its motion as it moved upward. Interstitial velocities were determined using neutrally buoyant polystyrene microcarrier beads (diameter 450 μm, Polysciences, Warrington, PA) as tracers. The Stokes number for the microcarriers was of the order of 0.03, and the concentration used was dilute (1 g/l), thus, the tracers could be assumed to follow the fluid closely.

The problem of light blockage by solids was resolved using transparent solid pieces. By closely matching the refractive indices of solid and liquid, the scatter at the interface was eliminated and

Table 1
Solid and liquid phase densities

Material	Density (kg/m^3)
Solution (1% CMC)	1004
Opaque solids	1060–1070
Acrylamide gels	1060–1070
Tracers	1004

measurements of tracer trajectories and velocities were then possible for high solid concentrations. In this experimental study, clear solid pieces were made from polyacrylamide gels (comprehensive preparation details have been presented by Zitoun, 1995), commonly used for electrophoresis. The density (Table 1) and physical properties of this gel closely resemble that of many common biomaterials, thus justifying the choice.

2.3.1. In-situ calibration

Determination of solid piece and tracer locations in three dimensions (3D) required a relationship between the image coordinates and real world coordinates. In order to account for camera and mirror misalignment, changes in the index of refraction which distorted the reflected image, and optical aberrations from lenses, we conducted an in-situ calibration on the actual setup field, and analyzed it just prior to experimentation. For the present experiment, a fiber optics matrix was used with known X, Y and Z coordinates (see Fig. 2 for more details). The calibration consisted of inserting a plexiglass plate with an array of 60 points made by using a plastic fiber light guide and illumination by using a fiber optic illuminator (Model 170D, Dolan Jenner, Rochester, NH). The real coordinates (X, Y, Z) and the image coordinates (X_1, Y_1) and (X_2, Y_2) from the left and right images, respectively, were correlated to relate the actual 3D positions to the (2D) locations in the two stereo views. The plate was moved to three different positions to map the whole area of interest (Fig. 3(a)). The array of points were videotaped at known locations and analyzed using the PTV algorithm to identify the location of the bright spots in the left and right views (Fig. 3(b)).

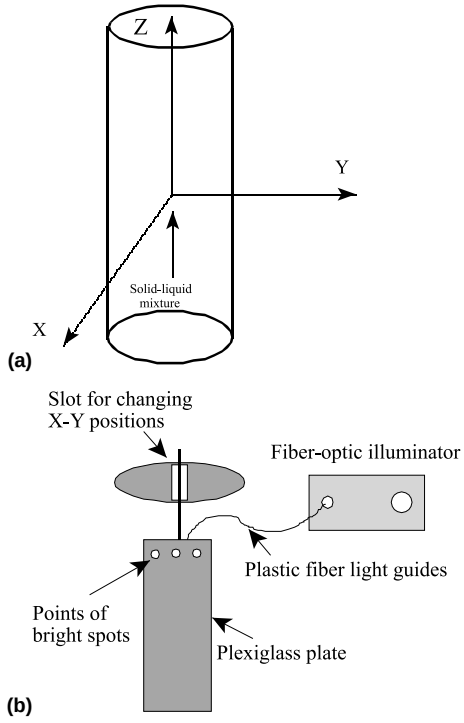

Fig. 2. (a) Coordinate system; (b) calibration apparatus.

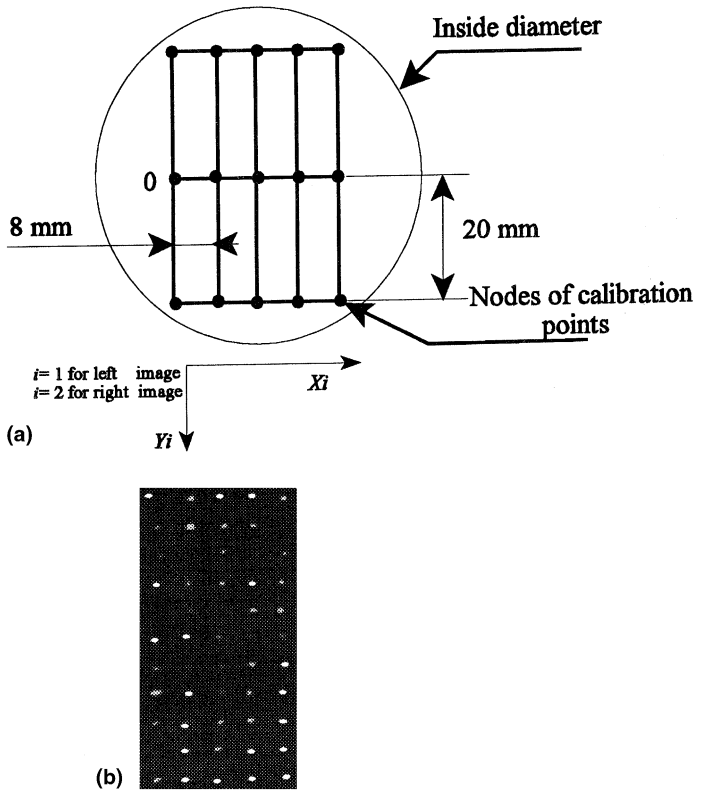

Fig. 3. (a) Map of points for in-situ calibration; (b) sample of calibration image using fiber optics wires.

2.3.2. Image processing

Each frame transferred from the frame grabber was first pre-processed to remove background and electronic noise, and improve image quality. Noise removal was achieved by using grey level thresholding (both high- and low-pass filtering). The image quality was further improved by generating a bilevel image which was formed by deciding a threshold level and setting all images above the threshold to be saturated and below it to be zero.

2.3.3. Details of image analysis

The image analysis was conducted after some modification of the algorithm written by Trigui et al. (1992) to obtain quantitative information from the images. Fig. 4(a) outlines the steps involved in the algorithm to determine the velocity vectors of two phases.

The algorithm located the particles and assigned a number for each particle, center location (X, Y), number of pixels spanned in the X and Y directions and the average light intensity. The frame-to-frame tracking was accomplished in two steps (Trigui et al., 1992): (l) the establishment of a search area and feasible particle trajectories and (2) a search for the actual particle path.

An estimate for the maximum anticipated particle travel distance was made from the knowledge of the system geometry, the flow conditions, the camera framing rate, and the length scale

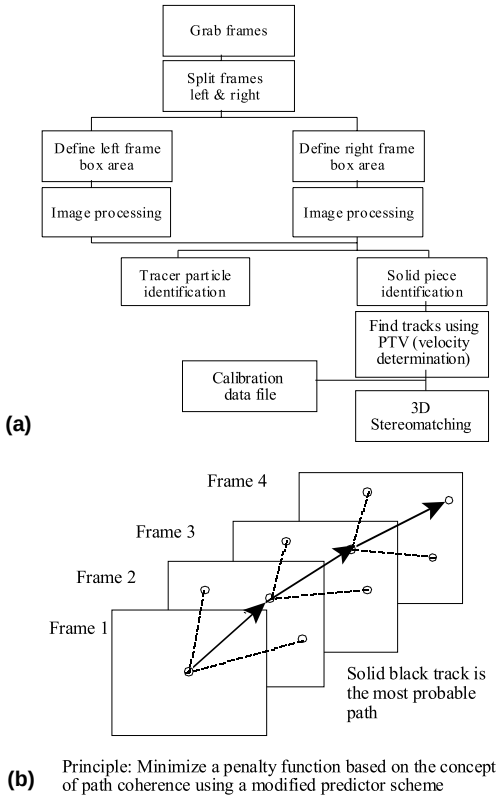

Fig. 4. (a) Steps of the PTV algorithm; (b) multi-frame tracking tree and technique.

ratio between the tube and the digitized images. The field of view was optimized to ensure that it was large enough for a sufficient number of frames to be accommodated to reconstruct trajectory and velocity information via PTV, yet small enough to maintain accuracy. After preliminary experimentation, it was decided to use a field of view of 10.5 cm.

Each particle was tracked through search areas within successive frames. Within each frame, the challenge consisted of identifying each particle with its counterpart in previous and successive frames. Since a given particle may take one of a number of possible paths, a rapidly growing "tree" of choices is set up, as illustrated in Fig. 4(b). Since the path, velocity and acceleration were all continuous and smooth functions, the procedure used was to look at each possible path in the tree and evaluate a penalty function that helped establish the most probable path (Fig. 4(b) shows more details). The penalty function was then compared for each possible branch in the search tree and the path associated with the lowest penalty function was retained as being the most likely physical path. A stereomatch corresponded to the intersection of the two optical rays which image the particle location in each view. The spatial locations of particle paths were found from the two-dimensional stereo pair particle trajectories. The displacements, velocity vectors, and their standard deviations for the particle paths were then evaluated. After obtaining the velocity vectors, particles with a stereomatching track represented the lowest of three penalty functions (one for each two-dimensional track and one for the stereomatching). The details of the three-dimensional

technique including penalty functions and procedures have been previously described by Guezennec et al. (1994) and Choi and Guezennec (1997).

The final data interpolation in conventional PTV, involves smoothing and presentation of velocity vector data over a regular grid by Adaptive Gaussian Window (AGW) interpolation (Spedding and Rignot, 1993; Garcia-Briones and Chalmers, 1994; Trigui et al., 1992). Successful interpolation requires the presence of sufficiently high tracer density to resolve local velocity variations. The more complex the flow, the greater the required density (e.g., highly developed turbulence). In the absence of the required tracer density, interpolation can result in erroneous flow information. In our experiments, the instantaneous velocity vector data were too sparse for the interpolation, and may have introduced errors larger than those involved in the image processing steps. We performed AGW to test its effectiveness, and determined errors from the AGW performance analysis curves presented by Spedding and Rignot (1993). Errors for our study ranged from 8.5% to 40%. Thus, we chose to retain our data as raw instantaneous velocity vectors instead of interpolated values.

An alternative approach to increasing data density up to 10 times is ensemble averaging, which is based on statistical averaging over several experiments, and has been used for mixing tanks (Yianneskis et al., 1987; Venkat et al., 1996). However, our interest was not in statistical averages, but instantaneous velocities; therefore, statistical averaging could not be used.

2.4. Experimental procedure: particle rotational motion and orientation distribution

The setup used was the same as that for the other experiments (Fig. 1), with the fluid–solid mixture being conveyed by air pressure from the inlet. The procedures were similar to those previously described with two notable modifications.

1. No polystyrene tracers were used, since the intent was to focus on solids behavior.
2. Two types of solid pieces were used: a limited number of opaque solids (which served as the objects of study), and a significant concentration of transparent (acrylamide gel) objects, which served as an optically unobtrusive high-concentration solid–liquid mixture. This enabled us to focus on the behavior of the opaque objects while ensuring that high solids concentrations were used. To clearly identify and image the rotation, all opaque solid objects had each face coated with a different color.

The analysis for this experiment was conducted differently from the previous experiment, and was based on the determination of Euler angles (θ, ψ and ϕ) for the solids over time during the flow. This was accomplished by finding three non-collinear unit vectors fixed on the solid particle when it moved with respect to a reference (camera axis) and time, and performing the analysis as detailed by Greenwood (1988).

2.5. Orientation distribution experiments

The experimental setup was the same as that for the rotation experiments; and the Euler angles were used for determination of orientation at any time. Since the most important parameter from our viewpoint was the orientation of the solids with respect to the tube axis, the Euler angles were transformed to one angle α, the orientation of the solid body's major axis with respect to the tube (Z) axis, as described by Zitoun (1995).

2.5.1. Statistical analysis

Orientation angles (α) were determined for the selected objects over the entire duration of their residence within the test section; and the mean values of α were determined in each case, to average out the effect of rotation. Distribution functions were based on of experiments involving sampling from 31 to 90 test objects. The orientation angles ranged from 0° to 90° for cylinders and from 0° to 45° for cubes, to avoid duplication of the angles that give the same cross-sectional area. Because of the symmetry of a cube, angles greater than 45° showed the same repeating pattern in area fraction as angles below 45°. Next, a frequency analysis of the angle α was conducted to determine the orientation distribution of the solids in continuous flow.

3. Results and discussion

The velocity field representation has been made in three orthogonal planes: XY, YZ and XZ, two axial planes (XZ, YZ) and one radial plane (XY). In the present discussion, we have limited our graphical presentation to the YZ and XY planes with respect to a range of X and Z interval values, respectively, rather than projections of all velocity vectors. The plots presented have the highest number of tracks in a specified plane.

3.1. Verification of accuracy

The accuracy of the velocity vectors was tested for a known velocity profile (single-phase flow) and the theoretical results compared with the experimental findings. The experimental values were close: the maximum deviation was 0.0009 m/s, which corresponds to 4.6% error.

3.2. Interstitial velocity

The influence of solid particles in a liquid medium is presented in Fig. 5 with experimental instantaneous raw velocity vectors in a two-dimensional projection the axial (YZ) plane field. Both the macroscopic and microscopic flow structures are time variant due to the intrinsic dynamic behavior of the dispersed solid-phase motion and associated wake interaction. Even though the flow regime is laminar (Re was varied from 9.4 to 26) all resemblance to a parabolic velocity profile vanished with the existence of solid pieces at high solid concentration. In Fig. 5, axial flow is dominant. The presence of the particles altered the velocity profiles of the carrier fluid in the three axes (X, Y and Z) due to the large momentum transfer between the two phases. Due to the relatively large solid size (8×16) and the high solid concentration (50%), solution and 50% cubic solid concentration (16×16 mm) at 1.577×10^{-4} m^3/s. the relative velocity between the two phases is also considerable. The fluid was forced to flow around solids, which increased the slip velocity between the liquid and solid phase. In all cases we found that on average, solids lagged the fluid velocity.

3.2.1. Fluid–solid relative velocity

Further analysis was also done to determine relative velocity by subtracting fluid velocity from the particle velocity found using the PTV algorithm. The solid pieces and tracer locations at each

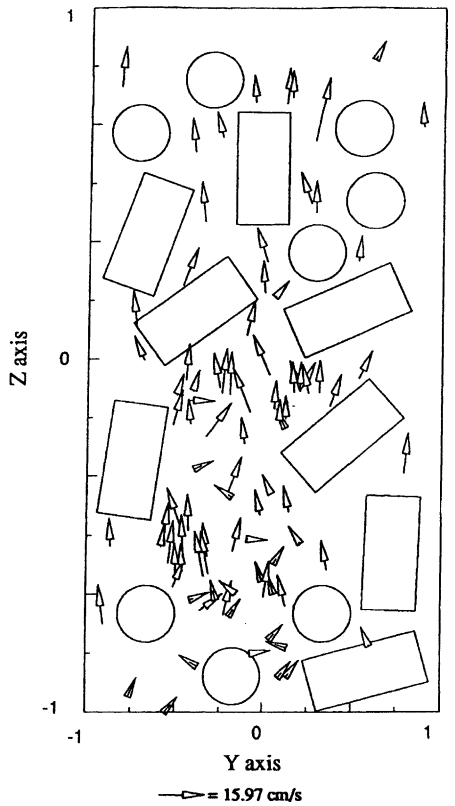

Fig. 5. Ranged raw instantaneous velocity vectors in *YZ* plane of CMC solution and 50% cylindrical solid concentration (8×16 mm) at 3.154×10^{-4} m^3/s (*Y* scale: 1 unit = 0.0508 m, *Z* scale: 1 unit = 0.1 m).

time (1/30 s) were stored in the data files and were sufficient to determine the relative velocity around the solid piece based on velocity vectors of both phases in the axial (*Z*) direction (the dominant flow direction). Only the instantaneous velocity vectors that were within a control volume 10% larger than the volume of particles were considered. The 10% was not based on the boundary layer thickness since the Reynolds number is relatively small which results in a thick boundary layer. Indeed in most cases, the boundary layer thickness was larger than the solid size and in that control volume, it was possible to accommodate another solid piece that may have interfered with the instantaneous velocity vectors. For this reason we limited our data to the vicinity of the particles by suggesting a control volume 10% greater than the particle size.

Increasing solid piece size increased relative velocity between phases as evidenced by comparison between Figs. 6(a) and (b). (Note that although the figures are for different shapes, the comparisons were consistent within the same shape). The figures in the radial (*XY*) plane show the radial dispersion of the velocity vectors. In Fig. 6, we can notice that the increase of solid concentration increases the dispersion of the fluid. However, it was observed that solid motion was restricted due to the interaction of solids during the flow. Notably, some parts in the figures were devoid of tracers. Since transparent solid pieces are similar in refractive index to fluid (they are nearly invisible) it is sometimes difficult to identify a solid piece except by absence of tracers.

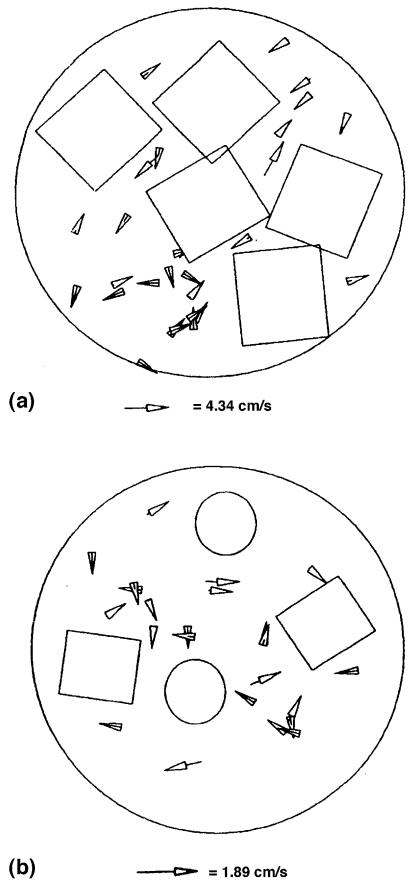

Fig. 6. Ranged raw instantaneous velocity vectors in the radial (XY) plane of CMC solution for: (a) 50% cubic solid concentration (16 mm) at 3.154×10^{-4} m^3/s; and (b) 30% solid concentration of cylindrical solids (8×8 mm) at 3.154×10^{-4} m^3/s (X and Y scales: 1:0.0254 m).

Figs. 7 and 8 illustrate relative velocities between solid and liquid. It is clear that the relative velocity in the axial (Z) direction is dominant. Some key observations regarding relative velocities were as follows.

As the flow rate increased the local relative velocity values significantly increased. The maximum and minimum values of the relative velocity ranged from 0.019 to 0.12 m/s for cubes and 0.0175 to 0.091 m/s for cylinders. Increasing the flow rate from 1.577×10^{-4} to 3.154×10^{-4} m^3/s at 30% solid concentration of 24 mm cubes increased relative velocity from 0.077 to 0.123 m/s. The same trend has been observed for 50% solid concentration but with lower values.

The increase of flow rate created unbalanced pressure equilibrium with respect to radial location of solids due to the tortuous path created by the random arrangements of solid pieces. This increased rotation of solids, specially cubes.

Increasing solid concentration played an important role in changing the velocity profile to a near-plug flow regime, which decreased the relative velocity. Increasing solid concentration from 30% to 50% decreased relative velocity for all cases. Eventually, the solid–liquid mixture behavior con-

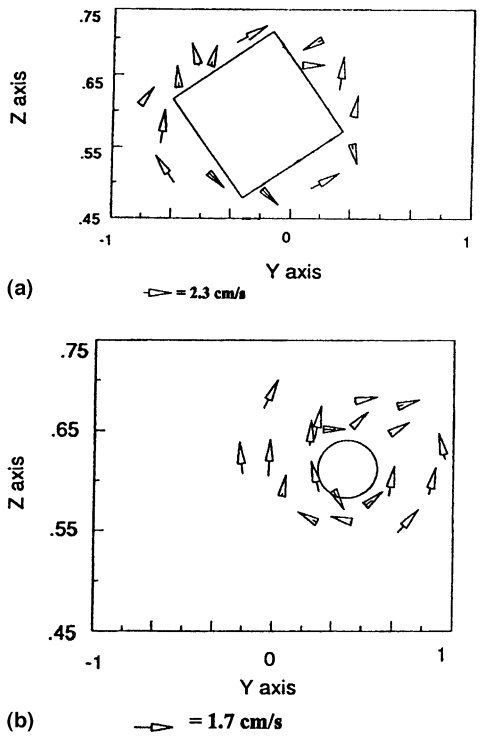

Fig. 7. Relative velocity between solid piece and fluid (CMC solution) in YZ plane at 50% solid concentration and 3.154×10^{-4} m^3/s: (a) cubic (24×24 mm); (b) cylindrical (8×16 mm), (Y scale: 1 unit $= 0.0508$ m, Z scale: 1 unit $=$ 0.1 m).

verges to a plug flow regime. The radial (XY) plots (Fig. 6) show that the longitudinal dispersion decreases by increasing the solid concentration. At high concentrations of solids (50%), particle interactions increase, with limited possibility for fluid motion. Hence, the relative velocity decreases.

Longitudinal mixing of solids is produced as a consequence of the complex movement of particles in the tube, especially due to solid to solid and wall to solid interactions. All data showed that cubes considerably affected the interstitial velocity. This phenomenon can be explained by observation of the solids motion. As the particles moved, wakes were formed behind them and interactions with other particles occurred. Both phenomena are responsible for the longitudinal mixing. Cubes showed a greater tendency to rotate than cylinders which creates mixing and disturbance of the flow. This observation has been noted more often at low solid concentration. During experiments the solid was observed to roll or slide against the wall or interact with other solids thereby decreasing its velocity. The higher ability for cubes to rotate and change coordinates and angles at low solid concentration can be explained by the presence of sharp edges and the packing of solids in the tube. For cylinders there are no sharp corners. When the curved surfaces of cylinders are in contact with the wall, the packing of smaller (8×8 mm) solids is higher than for cubes (8 mm side) and this results in less free space for solids to move. The decrease of free space limits solid rotation, and causes more interactions and collision with the wall. This tends to block the rotation in the three major axes, decreasing the mixing and therefore, the

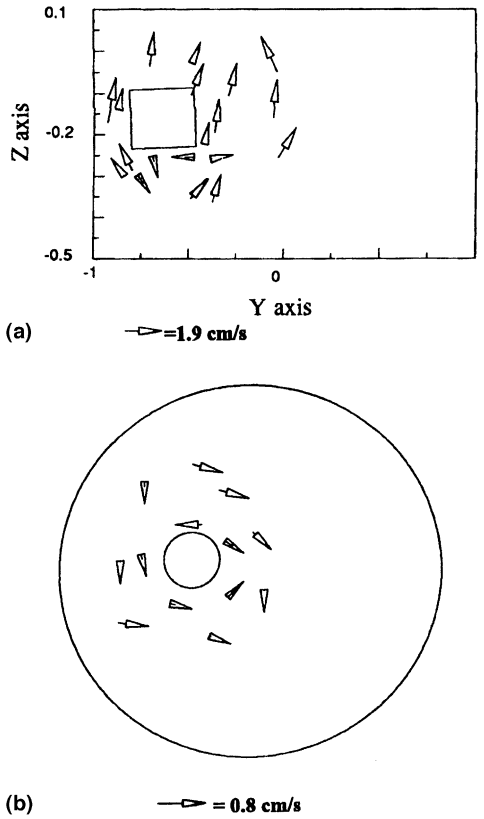

Fig. 8. Relative velocity vectors between solid and fluid: (a) cube in the axial (YZ) plane, and (b) cylinder in the radial (XY) plane at 30% solids concentration (16 mm) at 3.154×10^{-4} m^3/s. (X, Y scales: 1:0.0254 m, Z scale:1:0.05 m).

interstitial velocity. The two-phase flow and the sharp edges of the cubes complicate the configuration of the flow and create small eddies as the fluid flows in tortuous paths around the solid matrix. This induces mixing and recirculation (Fig. 8) of local fluid streams and axial dispersion of the fluid. It would be desirable to simulate such phenomena by direct numerical simulation in the manner of Hu (1996); however, the computation of colliding non-spherical particles is an issue that remains to be resolved.

The propensity of solid particles to cause fluid agitation and mixing also depended on the aspect ratio. Cylinders of 8×16 and 16×24 mm caused higher relative velocity compared to those of larger volume and unity aspect ratio. However, the tendency of longer solids to cause more mixing depended on the alignment of the major axis with the flow. As expected, solids had a tendency to rotate more frequently when the solid axis was perpendicular to the flow. However, in some cases, solids did not rotate at all even when the axis of the particle (1:2 aspect ratio) was perpendicular to the flow, when other solids in the vicinity prevented rotation. As a solid particle in a shear flow experiences hydrodynamic forces which cause pressure non-equilibrium and torques, causing the solid to rotate; this in turn will stir the fluid and promote dispersion. Based on our results the velocity gradients, particle shape, aspect ratio and solid concentration are critical factors for causing mixing.

This study demonstrates that it is possible to experimentally determine interstitial velocities in continuous flow of solid–liquid mixtures. The technique has been successfully adapted to determine local relative velocities between phases.

3.3. Solids rotation

3.3.1. Effect of size and aspect ratios

Increasing solid to tube size ratio decreased ($P < 0.01$) the rotation about all axes for both shapes, due apparently to increased interactions with the wall and with other solids. Also, increasing cylinder aspect ratio decreased ($P < 0.01$) the rotation due to their tendency to align with the flow (Fig. 9). High aspect ratio (1:3) solids have a tendency to align along their length, but those solids that are initially aligned across the flow will have a greater chance to rotate than low aspect ratio solids due to fluid-induced torque.

3.3.2. Effect of solid concentration

Rotation of solid particles decreased ($P < 0.01$) with an increase of solid fraction from 30% to 50% (Fig. 10). The increase of solid concentration increased the interactions between solids and decreased the free space available for free motion.

3.3.3. Effect of flow rate

Fig. 11 illustrates the effect of flow rate on rotation behavior on cubes. Increasing the flow rate from 1.577×10^{-4} and 3.154×10^{-4} m^3/s caused increasing flow disturbance. Even though the regime still was laminar we noticed a statistically significant increase ($P < 0.01$) of rotation. Higher torques would be expected by increasing the generalized Reynolds number from 9.4 to 26. Rotation about the x and y axes (axial plane) was greater than about the z axis (radial plane).

3.3.4. Effect of solid shape

The effect of shape on the rotation behavior was statistically significant ($P < 0.01$). Cubes rotated faster than cylinders, and this effect was more pronounced at lower solid concentration (Fig. 12). All data showed that cubes affect the rotation behavior considerably. This phenomenon may be due to the packing of particles in the tube. For cylinders the packing of smaller (8×8 mm)

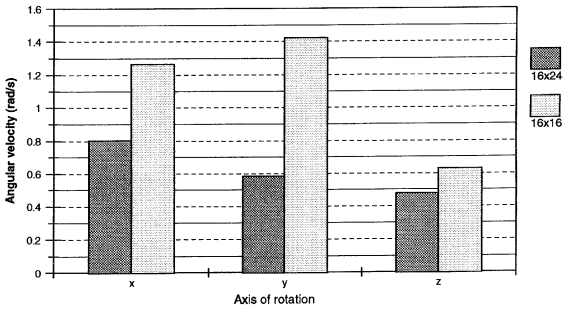

Fig. 9. Effect of aspect ratio on angular velocity about various axes at 30% solid concentration of cylinders at 3.154×10^{-4} m^3/s (16×16 and 16×24 mm in size).

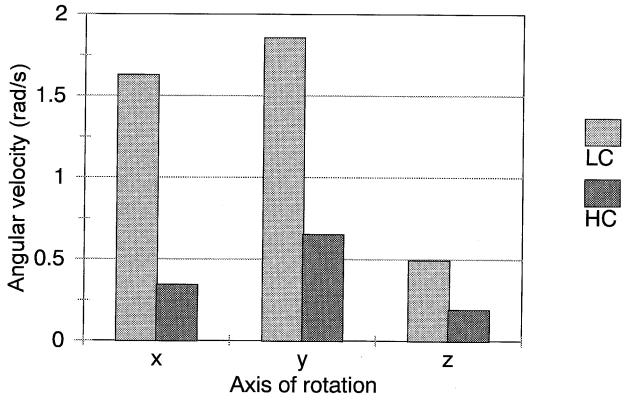

Fig. 10. Effect of solid concentration on angular velocity about various axes at 1577×10^{-4} m^3/s of cubes of 8×8 mm (LC and HC: 30% and 50% solid concentration, respectively).

solids is greater than for cubes (8 mm) which results in less free space for rotation, and causes more interactions and collisions with the wall. Even though cubes have a lower packing density than cylinders, they have a higher number of faces and edges, and therefore, a greater chance of interaction with the wall and with each other. The sharp edges of rectangular shapes apparently increase their tendency to rotate by increasing the probability of interacting with other solids. It was observed that cubes adjacent to the wall rotated more than cylinders, perhaps due to the discrepancy between the radii of curvature of the wall and the solids. Cases of non-rotation occurred mainly with cylinders. With cubes, such behavior was only temporary; particles soon started flipping and changing location and angles of orientation. The interstitial velocity study reported earlier showed deflection of velocity vectors due to wake effects and the sharp edges of cubes which may have caused local torques resulting in rotation. The sharp edges of the cubes complicated the configuration of the flow and created small eddies as the fluid flowed in tortuous paths created by the solid matrix. This induced mixing and recirculation of local fluid streams.

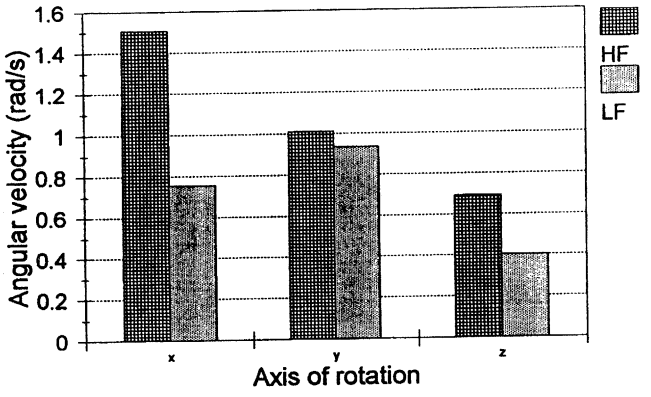

Fig. 11. Effect of flow rate on angular velocity about various axes at 30% solids concentration of cubes (24×24 mm) (LF = 1.577×10^{-4} m^3/s; HF = 3.154×10^{-4} m^3/s).

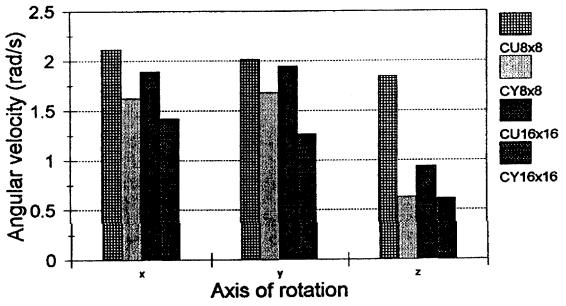

Fig. 12. Effect of solids shape on angular velocity about various axes at 30% solid concentration and 3.154×10^{-4} m^3/s. (CU = cube; CY = cylinder; 8×8 mm and 16×16 mm are the sizes of solids).

3.4. Solids orientation distribution

Figs. 13 and 14 present orientation distributions for cubic and cylindrical solids. Fig. 13 shows that increasing aspect ratio tended to align cylindrical solids with the flow direction, however, cubes showed no trend. The orientations were spread all over the range with no significant difference in magnitude (see Fig. 14). The effect of flow rate on orientation distribution was not clear. The only observation that can be mentioned is that the increase of flow rate increased the frequencies for angles between 60° and 90° for cylinders. This observation is due to the higher rotation of cubes compared to cylinders (as described under rotation). The sharp edges of cubes increased the rotation and therefore, orientation was affected by the shape. Because of the symmetry effect of a cubic solid when it rotates, orientation distribution of the angle α was relatively comparable in magnitude over the range 0° to 45° compared to cylinders where only one angle (0°–10°) was dominant.

The most frequently occurring orientations for cylinders were in line with the flow: 69% of cylinders were aligned with the flow (0°–10°), compared to only 25% of cubes. This observation can be supported by the decrease of rotation since the increase of aspect ratio, the increase of solid

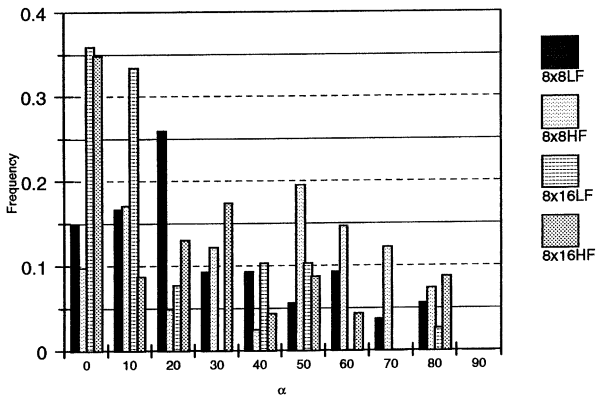

Fig. 13. Orientation (α) distribution for cylinders at 30% solid concentration (8×8 mm and 8×16 mm refers to diameter and length, respectively, LF and HF: refers to 1.577×10^{-4} m^3/s and 3.154×10^{-4} m^3/s flow rate, respectively).

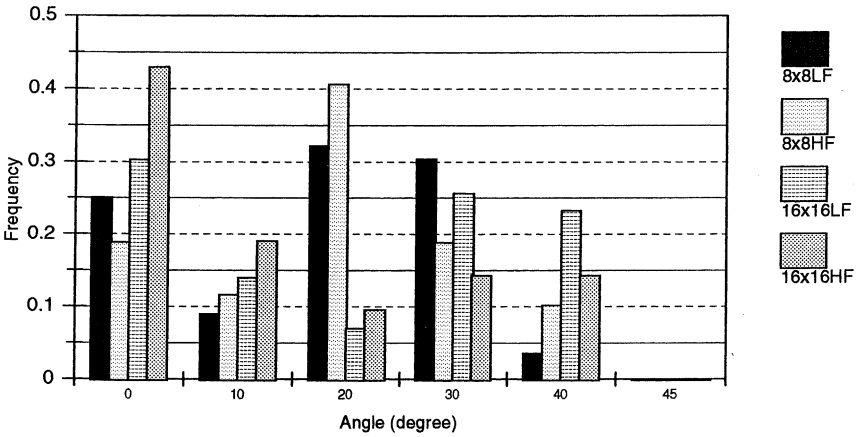

Fig. 14. Orientation (α) distribution for cubes at 30% solid concentration (8×8 mm and 16×16 mm refers to size diameter and length, respectively, LF and HF: refers to 1.577×10^{-4} m^3/s and 3.154×10^{-4} m^3/s flow rate, respectively

concentration and the absence of sharp edges for the cylinder increased the tendency of solids to align with the flow compared to cubes. The increase of the solids size (or solid to tube aspect ratio) showed that solids had a tendency to align with the flow.

4. Conclusions

Particle Tracking Velocimetry is a promising technique for velocity measurement, and can been adapted successfully for determination of interstitial velocities in the flow of solid–liquid mixtures. These studies reveal local slip velocity between phases that is dependent on solid piece shape and aspect ratio. However, the complexity of the flow necessitates the use of unprocessed velocity vector information, rather than a flow field interpolated onto a regular grid.

The PTV technique may be further modified to determine solid motions and orientation distribution of high solids suspensions, by determination of Euler angles. Our results demonstrate that objects of non-unity aspect ratio tend to align along the flow, within the constraints set by solids concentration, and that such solids also demonstrate decreased rotational motion in comparison with non-elongated solids. It is noted that elongated solids may rotate till an equilibrium position is achieved, whereupon no further rotation occurs. Our results also show that, as expected, increasing solids size and concentration decreases the incidence of rotation.

Acknowledgements

Research support of USDA NRICGP Grant No. 93-37500-9255 is gratefully acknowledged. Salaries and research support provided in part by OARDC, The Ohio State University. References to commercial products and trade names are made with the understanding that no endorsement or discrimination by The Ohio State University is implied.

References

Adrian, R.J., 1991. Particle imaging techniques for experimental fluid Mechanics. Annu. Rev. Fluid Mechanics 23, 261–304.

Altobeli, S.A., Gilver, R.C., Fukushima, E., 1991. Velocity and concentration measurements of suspensions by nuclear magnetic resonance imaging. J. Rheol. 35, 721–734.

Balasubramaniam, V.M., 1993. Liquid to particle convective heat transfer in aseptic processing systems. Ph.D. Dissertation. The Ohio State University.

Broadbent, C.J., Bridgwater, J., Parker, D.J., Keningley, S.T., Knight, P., 1993. A phenomenological study of a batch mixer using a positron camera. Powder Technol. 76, 317–329.

Chen, R.C., Fan, L.S., 1992. Particle image velocimetry for characterizing the flow structure in three-dimensional gas–liquid–solid fluidized beds. Chem. Eng. Sci. 47, 3615–3622.

Choi, W.-C., Guezennec, Y.G., 1997. In situ calibration for wide angle, 3-D stereoscopic image analysis. App. Optics 36, 7364–7373.

Garcia-Briones, M.A., Chalmers, J.J., 1994. Flow parameters associated with hydrodynamic cell injury. Biotechnol. Bioeng 44, 1089–1098.

Greenwood, D.T., 1988. Principles of Dynamics, second ed. Prentice Hall, Englewood Cliffs, NJ.

Guezennec, Y.G., Brodkey, R.S., Trigui, N., Kent, J.C., 1994. Fully automated three-dimensional PIV technique. Exp. in Fluids 17, 209–219.

Hu, H.H., 1996. Direct simulation of flows of solid-liquid mixtures. Int. J. Multiphase Flow 22, 335–352.

Larachi, F., Cassanello, M., Chaouki, J., Guy, C., 1995. Solids circulation patterns in three-phase fluidized beds containing binary mixtures of particles as inferred from γEPT. In: Proceedings of the Second International Conference in G-L and G-L-S reactor, Cambridge, UK.

Liu, Z.C., Adrian, R., 1993. Simultaneous imaging of the velocity filed in two phases. In: Roco, M. (Ed.), Particulate Two-phase Flow. Butter-worth-Heinemann, London, pp. 33–58.

Manavel, J.E., Powell, R.L., McCarthy, M.J., McCarthy, K.L., 1993. Magnetic resonance imaging of multiphase systems. In: Roco, M. (Ed.), Particulate Two-Phase Flow. Butterworth-Heinemann, Boston, pp. 127–140.

Meyer, M.J., Bethea, M.D., Guezennec, Y.G., Choi, W.-C., 1993. Stereo imaging velocimetry: a new option for microgravity experiments. In: Proceedings of ASME Meeting, New Orleans, November, 1993.

Orangi, S., Sastry, S.K., Li, Q., 1998. A numerical investigation of electroconductive heating of solid–liquid mixtures. Int. J. Heat Mass Transfer 41, 2211–2220.

Trigui, N., Guezennec, Y., Brodkey, R., 1992. Algorithms for fully automatic three dimensional particle image velocimetry. In: Proceedings of the 13th Symposium on Turbulence, University Missouri-Rolla (preprint).

Trigui, N., Kent, J.C., Guezennec, Y.G., Choi, W.C., 1994. Characterization of intake generated flow fields in I.C. engines using 3-D Particle Tracking Velocimetry, Paper 940279. In: Proceedings of the 1994 SAE International Congress, Detroit, March, 1994.

Sinton, S.W., Chow, A.W., 1991. NMR Flow imaging of fluids and solid suspensions in Poiseuille flow. J. Rheol. 35, 735–772.

Spedding, G.R., Rignot, E.J.M., 1993. Performance analysis and application of grid interpolation techniques for fluid flows. Exp. in Fluids 15, 417–430.

Venkat, R.V., Stock, R., Chalmers, J.J., 1996. Study of hydrodynamics in microcarrier culture spinner vessels: a particle tracking velocimetry approach. Biotechnology and Bioengineering 49, 456–466.

Yang, Y.B., Devanathan, N., Dukukovi, M.P., 1993. Liquid back mixing in bubble columns via computer-automated radioactive particle tracking (CARPT). Exp. in Fluids 16, 1–9.

Yianneskis, M., Popiolek, Z., Whitelaw, J.H., 1987. Structure of the trailing vortices around Rushton turbine blades. Trans. Instn. Chem. Engrs. A 71, 543–550.

Zitoun, K.B., 1992. Convective heat transfer coefficient between fluid and cubic particle in continuous tube flow. M.S. Thesis, The Ohio State University.

Zitoun, K.B., 1995. Continuous flow of solid-liquid mixtures during ohmic heating: fluid interstitial velocities, solid area fraction, orientation and rotation. Ph.D. Dissertation, The Ohio State University.